Published in final edited form as:

Cell. 2023 August 17; 186(17): 3632–3641.e10. doi:10.1016/j.cell.2023.06.026.

Structural basis for membrane-proximal proteolysis of substrates by ADAM10

Colin H. Lipper[1,2], **Emily D. Egan**[1], **Khal-Hentz Gabriel**[3], **Stephen C. Blacklow**[1,3,4,*]

[1]Department of Biological Chemistry and Molecular Pharmacology, Blavatnik Institute, Harvard Medical School, Boston, MA 02115, USA

[2]Current address: Seismic Therapeutic, Cambridge, MA 02142, USA

[3]Department of Cancer Biology, Dana Farber Cancer Institute, Boston, MA 02215, USA

[4]Lead Contact

Summary

The endopeptidase ADAM10 is a critical catalyst for regulated proteolysis of key drivers of mammalian development, physiology, and non-amyloidogenic cleavage of APP as the primary α-secretase. ADAM10 function requires formation of a complex with a C8-tetraspanin protein, but how tetraspanin binding enables positioning of the enzyme active site for membrane-proximal cleavage remains unknown. We present here a cryo-EM structure of a vFab-ADAM10-Tspan15 complex, which shows that Tspan15 binding relieves ADAM10 autoinhibition and acts as a molecular measuring stick to position the enzyme active site about 20 Å from the plasma membrane for membrane-proximal substrate cleavage. Cell-based assays of N-cadherin shedding establish that the positioning of the active site by the interface between the ADAM10 catalytic domain and the bound tetraspanin influences selection of the preferred cleavage site. Together, these studies reveal the molecular mechanism underlying ADAM10 proteolysis at membrane-proximal sites and offer a roadmap for its modulation in disease.

Graphical Abstract

*Correspondence: stephen_blacklow@hms.harvard.edu.

Author Contributions

Experimental Design: C.H.L., E.D.E., and S.C.B. Materials preparation: K-H.G., C.H.L. and E.D.E. Data acquisition: C.H.L. and E.D.E. Data analysis and interpretation: C.H.L. E.D.E., and S.C.B. Manuscript preparation and editing: C.H.L. and S.C.B. with input from E.D.E. Acquisition of Funding: S.C.B.

Inclusion and Diversity

One or more of the authors of this paper self-identifies as an underrepresented ethnic minority in their field of research or within their geographical location.

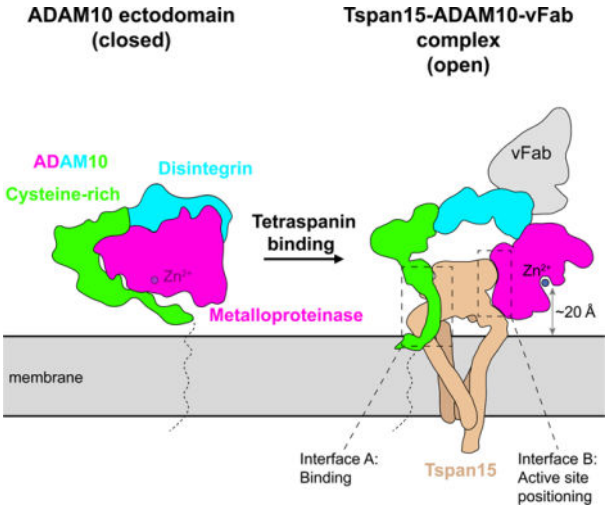

In brief

Membrane proximal proteolysis by ADAM10 depends on both relief of autoinhibition and distance measurement by its partner tetraspanin.

Introduction

Ectodomain shedding of transmembrane proteins plays a central role in a wide range of normal and pathophysiologic processes[1,2]. A Disintegrin and Metalloproteinase 10 (ADAM10) is a single-pass transmembrane protease that is essential in mammals[3], cleaving its substrates at membrane-proximal extracellular sites in a process called ectodomain shedding[4–7]. ADAM10 functions in physiological Notch signaling by catalyzing ligand-dependent Notch activation during development[8,9], and in pathologic Notch signaling in T-cell acute lymphoblastic leukemia[10], where oncogenic mutations result in dysregulated cleavage[11]. Additionally, ADAM10 processes a number of adhesion proteins including various cadherins, where cleavage is associated with both physiological and tumor cell migration[12–14], and Neuroligin-3, the shedding of which is indispensable for growth of high-grade gliomas[15]. ADAM10 also acts as an alpha-secretase in cleaving the amyloid precursor protein (APP) in a non-amyloidogenic manner, preventing toxic amyloid-beta generation by beta- and gamma- secretase cleavage[16,17]. Moreover, loss-off-unction mutations of ADAM10 are associated with an increased risk of developing Alzheimer's disease[18]. Thus, elucidating the molecular basis underlying cleavage of substrates by ADAM10 selectively at membrane-proximal sites is of general relevance to the pathogenesis of disease states as diverse as cancer and neurodegeneration.

ADAM10 is produced as an inactive zymogen, which matures into the active enzyme upon proprotein convertase-catalyzed release of its prodomain in the trans-Golgi network[19]. The structure of the mature ectodomain, which includes metalloproteinase, disintegrin, and cysteine-rich domains, revealed an autoinhibited conformation in which the cysteine-rich domain contacts the metalloproteinase domain, partially occluding access to the active site[20].

The maturation and function of ADAM10 are modulated by a class of proteins called tetraspanins, four-pass integral membrane proteins that have a vital role in organizing protein complexes in the membrane[21]. The six members of the TspanC8 subfamily (Tspan5, Tspan10, Tspan14, Tspan15, Tspan17, Tspan33; so named for their eight extracellular cysteines) are essential regulators of ADAM10[22], required for its maturation, trafficking, and subcellular localization[22–25]. Several studies suggest that TspanC8 proteins may also influence ADAM10 substrate specificity[23,26–31]. For example, Tspan15 promotes cleavage of N-cadherin (Ncad)[32], whereas Tspan5 and Tspan14 both favor cleavage of Notch receptors[23]. Tspan15-dependent N-cadherin cleavage is especially relevant to cancer progression and is associated with tumor cell invasion and metastasis[12,27,33,34], highlighting the role of Tspans as extrinsic factors in regulating ADAM10 cleavage activity, distinct from the intrinsic regulation imposed by selective binding pockets on the protease itself.

To elucidate how TspanC8 proteins recognize ADAM10 and understand how complex formation positions the ADAM10 active site proximal to the membrane for substrate cleavage, we determined the structure of a complex between Tspan15 and ADAM10 by cryo-EM, revealing an open conformation of ADAM10 positioned by the bound Tspan15 for efficient cleavage of transmembrane substrates at membrane-proximal positions. Our structural analysis and cell-based assays identify a molecular basis for ADAM10-catalyzed proteolysis selectively at membrane-proximal sites, showing that bound Tspan15 serves as a measuring stick to position the ADAM10 active site at a defined position relative to the plasma membrane.

Results

Structure of the ADAM10-Tspan15 complex

To facilitate structure determination, we first co-expressed ADAM10 and Tspan15 in HEK293F cells and extracted the ADAM10-Tspan15 complex into n-Dodecyl-β-D-Maltoside (DDM) – cholesterol hemisuccinate (CHS) detergent micelles. After affinity purification and exchange into glyco-diosgenin (GDN) – CHS, we then added an anti-ADAM10 11G2 Fab fragment, a fiducial marker for cryo-EM analysis and to increase complex mass. This Fab binds to the disintegrin domain of ADAM10 without perturbing the structure: in the x-ray structure of the complex of the 11G2 Fab with the soluble ADAM10 ectodomain, ADAM10 adopts the same closed conformation seen in the isolated ectodomain, the same closed conformation of the 11G2-ectodomain complex is also seen in negative stain EM images, and the bound 11G2 Fab does not alter the basal catalytic activity of the isolated, autoinhibited ectodomain[20]. We also included the metalloproteinase inhibitor BB94 during purification to prevent sample degradation from ADAM10 proteolytic activity. After isolating the full 11G2 Fab-ADAM10-Tspan15 complex by size-exclusion chromatography (Figure S1A–C, related to Figure 1) and confirming that the ADAM10-Tspan15 complex was catalytically active (Figure S1D, related to Figure 1), we determined the structure of the vFab-ADAM10-Tspan15 complex to 3.3 Å resolution using cryo-EM (Table 1 and Figure S2, related to Figure 1).

To build the initial model, the coordinates of the crystal structure of the ADAM10 ectodomain bound to the 11G2 Fab[20] and the alphafold2 model for Tspan15[35] were docked

into the cryo-EM electron density map. Whereas the Tspan15 model and the vFab portion of 11G2 fit readily into the density map, the ectodomain of ADAM10 did not. Instead, the catalytic domain and the disintegrin + cysteine-rich domains of ADAM10 were docked separately into the electron density before further refinement to produce a final model.

In the complex, the ADAM10 ectodomain adopts a C-shaped conformation encircling the Tspan15 ectodomain, and the two ectodomains are nestled together atop the four Tspan15 intramembrane helices which adopt a conical arrangement (Figure 1A,B). C-terminal to I670 of ADAM10, the transmembrane and cytoplasmic regions are not visible even when bound, presumably because they remain disordered in the complex. The variable domain of the 11G2 Fab (vFab) caps the complex at the N-terminal end of the ADAM10 distintegrin domain, distant from sites of ADAM10-Tspan15 contact.

The most striking feature of the structure is the conformational reorganization of ADAM10 upon complex formation with Tspan15. In the crystal structure of the isolated ADAM10 ectodomain, the protein is in a closed, autoinhibited conformation in which the metalloproteinase domain directly contacts the cysteine-rich domain[20] (Figure 1C, cartoon representation), whereas in the structure of the ADAM10-Tspan15 complex, ADAM10 is held in an open, active conformation by the large extracellular loop (LEL) of Tspan15, which interposes itself between the cysteine-rich and metalloproteinase domains (Figure 1B; see supplementary video S1 for a morph movie comparing the two conformations of ADAM10).

Tspan15, on the other hand, adopts a closed conformation in the complex, with its LEL sitting over the opening created by its four TM helices. This architecture resembles that of tetraspanins CD9[36], CD53[37] and CD81[38] in isolation (Figure S3, related to Figure 1), and differs from that of CD81 in complex with CD19, the only other bound-state structure of a tetraspanin: in the CD81-CD19 complex, the LEL undergoes a hinge movement to open up by 60° relative to the membrane plane, and the TM helices move closer together to occlude the intramembrane cavity[39].

Structure-function studies of the complex

The LEL domain of Tspan15 is wedged between the metalloproteinase and cysteine-rich domains of ADAM10, forming two discontinuous contact interfaces. The first, here called site A, is between Tspan15 and the ADAM10 cysteine-rich domain, and the second, site B, is between Tspan15 and the ADAM10 catalytic domain (Figure 2A, see Figure S4, related to Figure 2 for electron density of interface regions of each protein, and for the electron density of the bound active-site inhibitor BB94). Previous work has established that a complex still assembles in the absence of the catalytic domain, showing that the site B interface is not required for formation of the complex[32]. We therefore focused on mutationally interrogating site A to identify key contacts required for ADAM10 binding to Tspan15.

We introduced a series of mutations into ADAM10 at two patches in the site A interface and evaluated the effects of those changes on ADAM10-Tspan15 complex formation in a co-immunoprecipitation assay. The first patch, mutated at residues Y638/R646, alters a residue pair in contact with Tspan15 residues identified by mutation in a prior study

to contribute to ADAM10 binding[27]. The second mutation patch, P653/L654/R656, is in a short helix at the membrane surface that contacts the LEL, SEL and TM regions of Tspan15. We made two different sets of mutations in the first patch (Y638A/R646A and Y638E/R646E) and a triple alanine mutation in the second patch (P653A/L654A/R656A). Additionally, we made a five-Ala mutant combining the mutations in both patches (Y638A/R646A/P653A/L654A/R656A). Plasmids expressing Myc-tagged ADAM10 and FLAG-Tspan15 or empty vector were co-transfected into HEK293T cells, and cell lysates were subjected to co-immunoprecipitation as described previously[27] (Figure 2B). WT ADAM10 robustly immunoprecipitated with Tspan15 and showed increased conversion to the mature, processed form when co-transfected with Tspan15 compared to empty vector. Both Y638A/R646A and Y638E/R646E reduced the amount of ADAM that immunoprecipitated with Tspan15, and either reduced (Y638A/R646A) or prevented (Y638E/R646E) processing of ADAM10 into its mature form, respectively. The P653A/L654A/R656A protein failed to detectably co-immunoprecipitate with Tspan15, but retained the ability to undergo processing to the mature form. This observation suggests that this ADAM10 mutant is capable of an interaction (either a weak, transient association with Tspan15 or with another TspanC8) that supports its maturation into the mature form. The 5 Ala mutant (Y638A/R646A/P653A/L654A/R656A) neither immunoprecipitated with Tspan15 nor underwent processing to the mature form, indicating that it was both completely deficient in binding to Tspan15 and incapable of supporting ADAM10 maturation. The reduced Tspan15 abundance in the presence of the ADAM10 5 Ala mutant appears to be a consequence, not a cause, of its failure to interact with ADAM10: prior work has shown in other cell types that Tspan15 and ADAM10 are mutually stabilizing when bound (Eschenbrenner et al., 2020), that Tspan15 protein abundance is greatly diminished when not bound to ADAM10, or when co-expressed with ADAM10 in the presence of mutations fully disruptive of the ADAM10-Tspan15 interface[27], and that Tspan15 abundance is greatly decreased or undetectable in ADAM10 knockout cells[40]. Together, these data establish that Tspan15 binding and efficient ADAM10 maturation rely on contacts at the site A interface.

Constraints dictating membrane-proximal cleavage site selectivity

Although the site B interface does not control association of ADAM10 with Tspan15, it positions the active site Zinc ion ~20 Å from the membrane surface (Figure 3A). The active site cleft, occupied in our structure by the hydroxamic acid inhibitor BB94, is also oriented so that the C-terminal end of a bound substrate would be pointed toward the plasma membrane. These two structural features of the complex are consistent with the idea that Tspan15 binding constrains the position and orientation of the ADAM10 active site. For an unstructured 10-residue peptide, the radius of gyration would be approximately 20 Å ($R_g = nl^2/6$, where n=10 and the estimated Cα-Cα distance l ~ 3.8 Å); therefore, a 20 Å length constraint imposed by Tspan15 would result in preference for a cleavage position about 10 residues from the membrane, assuming that the segment between the membrane and the active site is natively disordered.

To test this idea, we varied the distance between the ADAM10 cleavage site and the membrane for the substrate N-cadherin (Ncad) and monitored the effects of changing the position of the processing site on the efficiency of cleavage by ADAM10. The wild-

type (WT) Ncad cleavage site is 10 residues from the plasma membrane. We designed a series of deletions and insertions in the membrane proximal region of Ncad to create variants with cleavage sites ranging from 6–18 residues from the membrane, along with a cleavage-resistant control mutant Ncad-GD[41] (Figure 3B). We analyzed the extent of Ncad cleavage of the different length variants in U251 cells, which rely on ADAM10 (Figure 3C) and Tspan15 for this processing event[27] (Figure 3D,E). The proteolysis results show that cleavage efficiency is optimal when the processing site is between eight and fourteen residues from the membrane. When the separation between the processing site and the membrane was shorter than nine residues, cleavage efficiency decreased, and when the distance was shortened to six residues (Ncad-4) processing was indistinguishable from the Ncad-GD cleavage resistant mutant (Figure 3D,E). As predicted from a random walk model, increasing the distance between the processing site and the membrane was better tolerated, with a four-residue insertion (Ncad+4) exerting no significant effect and only the eight-residue insertion (Ncad+8) showing a small, but significant, reduction in cleavage efficiency (Figure 3D,E).

Next, we tested whether site B is required for selective cleavage of the WT Ncad substrate by testing the effect of mutating Tspan15 residues at the site B interface (Figure 4A). Disruption of the site B interface with a trio of point mutations disfavors cleavage of the WT N-cad and further disfavors cleavage of shorter substrates without affecting cleavage of long substrates (Figure 4B,C), as predicted by a model in which site B tethers the ADAM10 active site proximal to the membrane.

We also examined whether different Tspan partners influenced the cleavage preference of ADAM10 by testing the effect of different Tspan-C8 proteins on cleavage of the Ncad, Ncad+4 and Ncad+8 substrates. Tspans 5, 14, 17, and 33 disfavor cleavage of the wild-type Ncad protein, and prefer to cleave the Ncad+4 and Ncad+8 longer substrates (Supplementary Figure S5A, related to Figures 3–5).

When cleavage of another known ADAM10 substrate, betacellulin, was investigated, Tspan15 directed ADAM10 cleavage to one site, whereas co-transfection of ADAM10 with Tspan5, albeit less efficiently, resulted in production of a higher molecular weight product and did not produce the shorter product formed with Tspan15 (Supplementary Figure S5B, related to Figures 3–5). Tspan10 appeared to be weakly permissive of inefficient cleavage at both sites, and other Tspan-C8 proteins did not promote detectable betacellulin cleavage.

The residues on Tspan15 at the contact interface with the metalloproteinase domain of ADAM10 vary among the six TspanC8 partner proteins that direct differential cleavage selectivity of ADAM10 for substrates (Figure 5A). In particular, Tspan5 and Tspan14 are divergent from Tspan15 in this region, have been shown to favor cleavage of Notch substrates, and disfavor cleavage of Ncad, suggesting that differences in this region among these TspanC8 proteins might alter positional selectivity of ADAM10 for substrate cleavage sites. To test this possibility, we designed chimeras of Tspan15 with Tspan5 and with Tspan14 that swap the sequence at the metalloprotease interface, spanning residues 206–230. The effect of these sequence swaps on N-cadherin cleavage was then analyzed using WT Ncad and the elongated Ncad+4 as substrates. Unlike Tspan15, which promoted

similar levels of cleavage for both WT Ncad and Ncad+4, the Tspan15-Tspan5 and Tspan15-Tspan14 chimeras exhibited impaired cleavage of Ncad while promoting cleavage of Ncad+4 more efficiently than the parental Tspan15 protein (Figure 5B,C). Consistent with the measuring-stick model, these results suggest that selectivity in substrate processing by distinct ADAM10-TspanC8 complexes might be tuned by the distance of the substrate cleavage site from the membrane.

Discussion

The structural and cell-based work reported here uncover the basis for intrinsic and extrinsic mechanisms that influence selection of a membrane proximal cleavage site by the alpha secretase ADAM10. In the structure of the isolated ectodomain, ADAM10 adopts a partially autoinhibited conformation and the active site of the catalytic domain has a deep hydrophobic pocket selective for bulky hydrophobic residues at the P1' position of the substrate[20]. In our cryo-EM structure of the Tspan15-ADAM10 complex, the bound Tspan15 converts ADAM10 into an open conformation and situates the catalytic site of the enzyme ~20 Å from the membrane surface, effectively creating a molecular ruler for cleavage at membrane proximal substrate sites.

The positioning of the ADAM10 catalytic site relative to the membrane is defined by the presence of two ADAM10-Tspan15 interfaces at site A and site B. Whereas the sequence at the site A interface is conserved among the C8 tetraspanins, the sequence at the site B interface is not. Some have proposed that complexation of ADAM10 with the six different C8-Tspan proteins creates six distinct molecular species with differential cleavage selectivity for substrates[42]. Among well characterized ADAM10 substrates, the ADAM10-Tspan15 complex selectively cleaves Ncad[32] and platelet glycoprotein (GP) VI[43], whereas Tspan5 and Tspan14 promote Notch processing by ADAM10[28,31]. In Ncad and GPVI, the P1' cleavage site is 10 residues from the membrane (note that misassignment of the start of the transmembrane region of GPVI by the Uniprot database has misled others[43] into stating that its cut site is five residues from the membrane, rather than 10), optimized for processing by ADAM10-Tspan15, whereas the separation of the cut site from the membrane is 15 residues for human Notch1[8]. While it is possible that different patterns of localization or direct substrate recruitment by different TspanC8 proteins account for some differences in the cleavage preferences of various ADAM10-TspanC8 complexes, our structural and proteolytic data suggest that differences in cleavage patterns among the six ADAM10-TspanC8 complexes can also result from differences in (or the absence of) the site B interface, which is not conserved among the TspanC8 proteins.

Modulation of ADAM10 activity has therapeutic potential for a number of human diseases ranging from Alzheimer's disease to cancer[11,15,44–46]. The development of therapeutics that act directly on ADAM10 has been challenging due to its numerous physiological substrates and the subsequent on-pathway toxicity that results from altering their processing[47]. Our findings open up the possibility of selectively inhibiting or activating cleavage of a distinct target protein such as Notch1 or APP using an antibody directed at a specific TspanC8 protein, analogous to the modulation of CD19-CD81 complexation in B cell co-receptor signaling with an antibody directed at the Tspan CD81[48]. Promisingly, the

anti-Tspan15 antibody 1C12 was able to bind Tspan15 when in complex with ADAM10 and displayed a partial inhibitory effect on ADAM10 cleavage of VE-cadherin in a cell-based assay[40]. When superimposed on the ADAM10-Tspan15 complex structure reported here, our structure of the 1C12 Fab bound to the Tspan15 LEL[27] shows that the Fab would clash with the disintegrin and metalloproteinase domains (Supplementary Figure S6, related to Figures 3–5), indicating that the antibody likely displaces the catalytic domain of ADAM10 from Tspan15 to interfere with VE-cadherin cleavage. Development of TspanC8-directed antibodies targeting the site B interface could be developed to modulate ADAM0 substrate selectivity for therapeutic applications, such as to promote alpha-secretase cleavage of APP. Other antibodies that promote or inhibit the activity of distinct ADAM10-TspanC8 complexes should enable specificity in modulating ADAM10 activity toward other desired substrates (*e.g.* Notch, N-cadherin) while reducing the undesired consequences of modulatory antibodies or compounds that directly activate or inhibit ADAM10.

Limitations of the Study

One caveat to note is that our structure was determined in detergent, not in the presence of membrane lipids or in an intact bilayer. Although we did show that the complex is active in cleaving a fluorogenic peptide substrate in the identical buffer to that used for structure determination, our studies do not provide any information about potential structural roles for lipids in complex formation or stabilization of either the primary (site A) or secondary (site B) interface. In addition, the transmembrane portion of ADAM10 was also not visible in the structure, and it is possible that this region becomes ordered in the natural microenvironment of the membrane. The sequence contexts and conformational preferences of different substrates in their membrane-proximal regions likely also exert an influence on ADAM10 cleavage sensitivity, and our studies did not evaluate structural features of the substrates in this region. Another limitation we encountered was that it was not possible to test the Tspan15 length-dependence for cleavage of APP and Notch substrates in our U251 cell-based assay system because there was a high amount of basal cleavage activity toward those substrates even in Tspan15 knockout cells. As a result, understanding how the different Tspan-C8 proteins might influence substrate selectivity will still require further analyses. Nevertheless, our studies provide a clear structural rationale for the length constraint in cleavage at membrane-proximal sites by ADAM10-Tspan15 complexes.

STAR Methods

Resource availability

Lead contact—Further information and requests for either resources or reagents should be directed to and will be fulfilled by the lead contact Stephen C. Blacklow (stephen_blacklow@hms.harvard.edu).

Materials availability—Requests for materials generated in this study should be directed to and will be fulfilled by the lead contact Stephen C. Blacklow (stephen_blacklow@hms.harvard.edu).

Data and Code Availability—The coordinates of the 11G2 vFab-ADAM10-Tspan15 complex have PDB ID code 8ESV and the EM map has EMDB accession number EMD-28580. Other materials are available upon request to S.C.B. This paper does not report original code. Any additional information required to reanalyze the data reported in this paper is available from the lead contact upon request.

Experimental model and study participant details

Protein for cryo-EM was isolated from Expi293F cells. Expi293 cells were maintained in suspension at 37°C, 8% CO_2 in Expi293 expression medium (ThermoFisher). Co-immunoprecipitation experiments were performed in HEK293T cells. N-cadherin cleavage assays were performed in U251 cells. HEK293T and U251 cells were maintained at 37°C in DMEM (Corning) supplemented with 10% fetal bovine serum (GeminiBio) and penicillin/streptomycin (Gibco).

Method details

Plasmid construction—ADAM10 used for structure determination was expressed using a modified version of the PRK5M-ADAM10 plasmid (Addgene plasmid 31717) with a FLAG tag immediately following the prodomain boundary site and the myc tag removed (FLAG-ADAM10). Tspan15 was cloned into pcDNA3.1/Hygro(+) with an N-terminal 6-histidine tag followed by an enterokinase cleavage site (used as a linker, His-EK-Tspan15). A single DNA insert containing the 11G2 light chain followed by a P2A ribosomal skipping sequence and then the heavy chain Fab sequence was inserted into the pFUSE-hIgG1-Fc2 plasmid containing the human IgG Fc. The sequence contains a 3C protease site between the light chain and the P2A sequence, and another 3C site between the heavy chain and the Fc. The light chain uses the IL2 signal sequence in the vector and the heavy chain uses the native signal sequence. 11G2 contains the N79Q mutation in the heavy chain to remove a glycosylation site. N-cadherin wild-type and mutant sequences were cloned into pcDNA3.1/Hygro(+) with a C-terminal HA tag. Tspan15-Tspan5 and Tspan15-Tspan14 chimeras replace Tspan15 residues 206–230 with Tspan5 residues 208–232 and Tspan14 residues 208–232, respectively. These constructs as well as wild-type Tspan15 were inserted into pcDNA3.1/Hygro(+) with an N-terminal FLAG tag. Co-immunoprecipitation and N-cadherin cleavage assays used FLAG-Tspan15 constructs and ADAM10-myc constructs (Addgene plasmid 31717 and point mutants derived from it).

Protein expression—All proteins were expressed in Expi293F cells. Cells were grown in Expi293 growth medium to a density of 3.0×10^6 cells/mL and then transfected with 1.0 mg DNA / L of culture using PEI MAX 40K reagent at a 1:3 DNA/PEI ratio. 24 hours after transfection 10 mL per L culture of 45% D-(+)-Glucose solution (Sigma-Aldrich) and 3 mM valproic acid sodium salt (Sigma-Aldrich) were added to the cells. For expression of the ADAM10-Tspan15 complex, cells were co-transfected with each plasmid in a 1:1 ratio and cells were incubated for 48 hours after transfection before harvesting. For 11G2 antibody expression, cells were incubated for 5–6 days after transfection before the antibody was recovered from the media.

11G2 Fab purification—Conditioned media containing 11G2 antibody was passed over Protein A agarose. The retained protein was washed with buffer containing 20 mM HEPES pH 7.4 and 150 mM NaCl. The antibody was eluted with buffer containing 20 mM glycine pH 3.0 and 150 mM NaCl, then neutralized by adding 1 M HEPES, pH 7.4 to a final buffer concentration of 100 mM. The Fc was released from the Fab by adding 3C protease at a ratio of 1:40 (w/w) and incubating at room temperature overnight. The Fc was then removed from the solution by passage over Protein A resin.

ADAM10-Tspan15 complex purification—Cells expressing ADAM10 and Tspan15 were harvested by centrifugation and lysed by osmotic shock in 20 mM HEPES pH 7.4, containing 2 mM MgCl2, 10 μM ZnCl2, 1 mM CaCl2, 2 mg/ml iodoacetamide (Sigma Aldrich), 1:50,000 (v:v) benzonase nuclease, and 1 μM BB94. Lysed cells were then centrifuged at 50,000 × g for 20 minutes. The ADAM10-Tspan15 complex was then extracted in buffer containing 20 mM HEPES pH 7.4, 150 mM NaCl, 10 % (v/v) glycerol, 1% (w/v) n-Dodecyl-β-D-Maltoside (DDM), 0.1% (w/v) cholesteryl hemisuccinate (CHS), 2 mg/ml iodoacetamide, 10 μM ZnCl2, 5 mM CaCl2 and 1 μM BB94 using a glass Dounce homogenizer, then stirred for 1 h at 4 °C. Extracted protein was centrifuged at 50,000 × g for 30 minutes. Supernatant was loaded onto a column containing 3 ml M1 FLAG resin, washed with 10 ml of 20 mM HEPES pH 7.4, containing 150 mM NaCl, 1 % glycerol, 0.1% DDM, 0.01% CHS, 5 mM CaCl2, and 1 μM BB94, then washed with 40 ml of 20 mM HEPES pH 7.4, containing 150 mM NaCl, 0.03% GDN, 0.003% CHS, 5 mM CaCl2, and 1 μM BB94. Protein was eluted with 0.2 mg/ml FLAG peptide in 20 mM HEPES pH 7.4, containing 150 mM NaCl, 0.03% GDN, 0.003% CHS, and 1 μM BB94. Eluted protein was then added to Ni-NTA resin and washed with 20 mM HEPES pH 7.4, containing 150 mM NaCl, 0.03% GDN, 0.003% CHS, 20 mM imidazole, and 1 μM BB94. Protein was eluted with the same buffer containing 250 mM imidazole. The ADAM10-Tspan15 complex was incubated with excess 11G2 Fab for 1 h and further purified by size-exclusion chromatography using a Superdex 200 Increase 10/300 GL column in 20 mM HEPES pH 7.4, containing 150 mM NaCl, 0.03% GDN, and 0.003% CHS. ADAM10-Tspan15 used for enzymatic analysis was purified without the addition of BB94 and 11G2 Fab, with final buffer conditions of 20 mM HEPES pH 7.4, 150 mM NaCl, 0.03% GDN, 0.003% CHS, and 2 μM ZnCl2.

Fluorogenic peptide cleavage assay—The reaction was initiated by mixing ADAM10-Tspan15 complex (final concentration 0.5 μM) with 25 μM fluorogenic peptide substrate, Mca-PLAQAV-Dpa (R&D Systems) at 37 °C. The reaction buffer consisted of 20 mM HEPES pH 7.4, 150 mM NaCl, 0.03% GDN, 0.003% CHS, and 2 μM ZnCl2. The reaction was monitored by fluorescence emission (excitation = 320 nm and emission = 405 nm) using a SpectraMax M5 Microplate Reader (Molecular Devices). Data were analyzed using Graphpad Prism software. Two replicates were performed.

Cryo-EM grid preparation—Quantifoil holey carbon film-coated 400 mesh copper grids (Electron Microscopy Sciences, R1.2/1.3) were glow discharged using a PELCO easiGlow (Ted Pella) for 30 s at 15 mA. A Vitrobot Mark IV was used for sample application and plunge-freezing. 3.3 μl of 2.1 mg/ml ADAM10-Tspan15–11G2 was applied to each grid at

22 °C with 100% humidity, followed by blotting for 7 s with a blot force of 15. The grids were then plunge-frozen in liquid ethane and stored in liquid nitrogen until data collection.

Cryo-EM data collection—Grids were imaged on a FEI Titan Krios operated at 300 kV with a K3 summit direct electron detector camera in counting mode. Data were acquired at a nominal magnification of 105,000x, pixel size of 0.825 Å, total exposure dose of 51.99 $e^{-}/Å^2$ over 50 frames and 1.04 $e^{-}/Å^2$ dose per frame. A total of 10037 movies were collected with a defocus in the range of −1.0 and −2.2 μm.

Cryo-EM data processing and model building—Data were processed using CryoSPARC[52]. Movies were motion-corrected using patch motion correcting and contrast transfer function (CTF) parameters were estimated using patch CTF estimation. Micrographs were then curated to exclude those with CTF resolution below 4.5 Å, resulting in 8653 micrographs used. A 3-dimensional model from a small dataset collected previously on a Talos Arctica was used to make 30 2-dimensional templates that were used for template-based picking in CryoSPARC. 1822048 initial particles were picked. Particles were selected using three rounds of 2-D classification resulting in 452065 particles. Four ab-initio models were produced, then three rounds heterogeneous refinement were used for further particle selection, producing a final set of 178031 particles. Non-uniform refinement performed using this particle set and the best model from heterogeneous refinement produced a map at 3.4 Å. Then local refinement was performed using a mask that excluded the constant region of the 11G2 Fab, resulting in a map at 3.3 Å resolution. The map was post-processed with DeepEMhancer using the highRes model[53]. Atomic coordinates for ADAM10 (PDB 6BE6), 11G2 Fab (PDB 6BDZ) and the predicted structure for Tspan15 (Alphafold database O95858) were fit into the density using Chimera[54]. Due to the structural reorganization of ADAM10, the coordinates (PDB 6BE6) were divided into two parts for fitting: the metalloproteinase domain and the disintegrin-cysteine-rich region. The model was built in Coot[56] and refined in Phenix Real-Space Refine[55] using secondary structure restraints. Model to map FSC was produced using Phenix Comprehensive Validation.

Co-immunoprecipitation and western blotting—HEK293T cells were grown in 6 well tissue culture dishes in DMEM with 10% FBS and transfected with 2 μg DNA per well (1 μg each of ADAM10-myc and FLAG-Tspan15 plasmids) using Fugene HD (Promega) transfection reagent. DNA and reagent were mixed at a 1:3 DNA/Fugene HD ratio in Opti-MEM media (150 μl per well), incubated for 15 minutes then added to the cells. Cells were incubated for 48 hours, then washed in ice cold PBS and lysed in buffer containing 20 mM HEPES pH 7.4, 150 mM NaCl, 1% DDM and 10 μM BB94. Lysed cells were then centrifuged at 20000 × g for 10 minutes. Lysates were added to 20 μl of M2 anti-FLAG resin and incubated for one hour at 4 °C. The resin was washed three times with buffer containing 20 mM HEPES pH 7.4, 150 mM NaCl, 0.1% DDM and 1 μM BB94. 2X SDS loading dye was added directly to the washed resin. Samples were run on an SDS-PAGE gel, and transferred to a nitrocellulose membrane. Membranes were blocked in tris-buffered saline containing 0.1% Tween 20 (TBST) containing 5% non-fat milk for one hour, and then incubated in primary antibody overnight at 4 °C. Membranes were washed three times with

TBST and incubated with secondary antibody for one hour at room temperature. Membranes were washed three times with TBST and blots were developed using Western Lightning Plus-ECL detection Kit. Primary antibodies used for western blotting were anti-FLAG (Cell Signaling Technology; rabbit, 1:2000 dilution), anti-myc (Cell Signaling Technology; rabbit, 1:2000 dilution), and anti-GAPDH (Cell Signaling Technology; rabbit, 1:2000 dilution). Anti-rabbit-HRP (Abcam) was used for the secondary antibody at 1:10000. Two biological replicates were performed.

N-cadherin cleavage assay—U251 Tspan15 knockout cells were reported previously[27]. U251 wild-type cells and Tspan15 knockout cells were grown in 6 well tissue culture dishes in DMEM with 10% FBS. Cells were transfected with 2 μg total DNA (2 μg Ncad-HA plasmid for Figure 3; 1 ug each Ncad-HA and FLAG-Tspan plasmids for Figures 4 and 5) using 3.2 μl U251 Avalanche transfection reagent (EZ Biosystems). 48 hours after transfection, fresh media containing the gamma-secretase inhibitor compound E (500 nM) was added to the cells. After one hour, 2 μM N-ethylmaleimide (NEM) was added to the cells. 40 minutes after adding NEM, the cells were washed in PBS and lysed directly in 500 μl SDS-loading dye containing 5% β-mercaptoethanol and 2 mM EDTA. Samples were sonicated and run on an SDS-PAGE gel. Proteins were then transferred to a nitrocellulose membrane. Membranes were blocked in TBST containing 5% non-fat milk for one hour before incubation with primary antibodies overnight at 4 degrees C. Primary antibodies used were anti-HA antibody (Cell Signaling Technology; mouse, 1:1000 dilution), anti-FLAG (Cell Signaling Technology; rabbit, 1:2000 dilution), anti-β-tubulin (Cell Signaling Technology; mouse, 1:1000 dilution), or GAPDH (Cell Signaling Technology; rabbit, 1:5000). Membranes were washed three times with TBST and incubated with anti-rabbit-HRP (Abcam; 1:10000 dilution) or anti-mouse-HRP (ThermoFisher; 1:10000 dilution) for one hour. Membranes were again washed three times with TBST. Western blots were developed using Western Lightning Plus-ECL detection Kit (PerkinElmer)[27]. Blots were quantified using ImageJ software. Statistical analysis was performed in GraphPad Prism 7 using an unpaired t test (two-tailed). Three biological replicates were performed.

Quantification and Statistical Analysis

Results of statistical analyses are found in the results section of the main text and in the figure legends for Figures 3–5. Data shown for the western blots quantified in Figures 3–5 are representative of 3 independent experiments (n=3). All calculations of significance were determined using GraphPad Prism 7 software using an unpaired t test (two-tailed). Data are reported as mean ± standard deviation. Significance was determined by a p value of < 0.05, and annotated as $*P < 0.05$, $**P < 0.01$, and, where indicated, $***P < 0.001$.

Supplementary Material

Refer to Web version on PubMed Central for supplementary material.

Acknowledgments

We thank the cryo-EM Center for Structural Biology at Harvard Medical School for expert assistance with cryo-EM data acquisition and processing, Lena Tveriakhina for preparation of the graphical abstract, and members of the

Blacklow lab for helpful discussions. Financial support for this work was provided by NCI grants R35 CA220340 and R01 AI172846 (to S.C.B.), and a gift from Edward B. Goodnow (to S.C.B.).

Declaration of Interests

S.C.B. is on the board of the non-profit Institute for Protein Innovation, on the board of the non-profit Revson Foundation, and on the scientific advisory board for and receiving funding from Erasca, Inc. for an unrelated project. He is an advisor to MPM Capital, and a consultant for IFM, Scorpion Therapeutics, Odyssey Therapeutics, Droia Ventures, and Ayala Pharmaceuticals for unrelated projects. C.H.L. is currently an employee of Seismic Therapeutic.

References

1. Lichtenthaler SF, Lemberg MK, and Fluhrer R (2018). Proteolytic ectodomain shedding of membrane proteins in mammals—hardware, concepts, and recent developments. EMBO J. 37. 10.15252/embj.201899456.
2. Peschon JJ, Slack JL, Reddy P, Stocking KL, Sunnarborg SW, Lee DC, Russell WE, Castner BJ, Johnson RS, Fitzner JN, et al. (1998). An Essential Role for Ectodomain Shedding in Mammalian Development. Science. 10.1126/science.282.5392.1281.
3. Hartmann D, de Strooper B, Serneels L, Craessaerts K, Herreman A, Annaert W, Umans L, Lübke T, Lena Illert A, von Figura K, et al. (2002). The disintegrin/metalloprotease ADAM 10 is essential for Notch signalling but not for α-secretase activity in fibroblasts. Hum. Mol. Genet 11, 2615–2624. 10.1093/hmg/11.21.2615. [PubMed: 12354787]
4. Kuhn P-H, Colombo AV, Schusser B, Dreymueller D, Wetzel S, Schepers U, Herber J, Ludwig A, Kremmer E, Montag D, et al. (2016). Systematic substrate identification indicates a central role for the metalloprotease ADAM10 in axon targeting and synapse function. eLife 5, e12748. 10.7554/eLife.12748. [PubMed: 26802628]
5. Lambrecht BN, Vanderkerken M, and Hammad H (2018). The emerging role of ADAM metalloproteinases in immunity. Nat. Rev. Immunol 18, 745–758. 10.1038/s41577-018-0068-5. [PubMed: 30242265]
6. Pruessmeyer J, and Ludwig A (2009). The good, the bad and the ugly substrates for ADAM10 and ADAM17 in brain pathology, inflammation and cancer. Semin. Cell Dev. Biol 20, 164–174. 10.1016/j.semcdb.2008.09.005. [PubMed: 18951988]
7. Weskamp G, Ford JW, Sturgill J, Martin S, Docherty AJP, Swendeman S, Broadway N, Hartmann D, Saftig P, Umland S, et al. (2006). ADAM10 is a principal “sheddase” of the low-affinity immunoglobulin E receptor CD23. Nat. Immunol 7, 1293–1298. 10.1038/ni1399. [PubMed: 17072319]
8. Mumm JS, Schroeter EH, Saxena MT, Griesemer A, Tian X, Pan DJ, Ray WJ, and Kopan R (2000). A ligand-induced extracellular cleavage regulates gamma-secretase-like proteolytic activation of Notch1. Mol. Cell 5, 197–206. 10.1016/s1097-2765(00)80416-5. [PubMed: 10882062]
9. Sprinzak D, and Blacklow SC (2021). Biophysics of Notch Signaling. Annu. Rev. Biophys 10.1146/annurev-biophys-101920-082204.
10. Weng AP, Ferrando AA, Lee W, Morris JP, Silverman LB, Sanchez-Irizarry C, Blacklow SC, Look AT, and Aster JC (2004). Activating mutations of NOTCH1 in human T cell acute lymphoblastic leukemia. Science 306, 269–271. 10.1126/science.1102160. [PubMed: 15472075]
11. Sulis ML, Saftig P, and Ferrando AA (2011). Redundancy and specificity of the metalloprotease system mediating oncogenic NOTCH1 activation in T-ALL. Leukemia 25, 1564–1569. 10.1038/leu.2011.130. [PubMed: 21625236]
12. Kohutek ZA, diPierro CG, Redpath GT, and Hussaini IM (2009). ADAM-10-Mediated N-Cadherin Cleavage Is Protein Kinase C- Dependent and Promotes Glioblastoma Cell Migration. J. Neurosci 29, 4605–4615. 10.1523/JNEUROSCI.5126-08.2009. [PubMed: 19357285]
13. Maretzky T, Reiss K, Ludwig A, Buchholz J, Scholz F, Proksch E, Strooper B. de, Hartmann D, and Saftig P (2005). ADAM10 mediates E-cadherin shedding and regulates epithelial cell-cell adhesion, migration, and β-catenin translocation. Proc. Natl. Acad. Sci 102, 9182–9187. 10.1073/pnas.0500918102. [PubMed: 15958533]

14. Solanas G, Cortina C, Sevillano M, and Batlle E (2011). Cleavage of E-cadherin by ADAM10 mediates epithelial cell sorting downstream of EphB signalling. Nat. Cell Biol 13, 1100–1107. 10.1038/ncb2298. [PubMed: 21804545]
15. Venkatesh HS, Tam LT, Woo PJ, Lennon J, Nagaraja S, Gillespie SM, Ni J, Duveau DY, Morris PJ, Zhao JJ, et al. (2017). Targeting neuronal activity-regulated neuroligin-3 dependency in high-grade glioma. Nature 549, 533–537. 10.1038/nature24014. [PubMed: 28959975]
16. Esler WP, and Wolfe MS (2001). A Portrait of Alzheimer Secretases--New Features and Familiar Faces. Science. 10.1126/science.1064638.
17. Kuhn P-H, Wang H, Dislich B, Colombo A, Zeitschel U, Ellwart JW, Kremmer E, Roßner S, and Lichtenthaler SF (2010). ADAM10 is the physiologically relevant, constitutive α-secretase of the amyloid precursor protein in primary neurons. EMBO J. 29, 3020–3032. 10.1038/emboj.2010.167. [PubMed: 20676056]
18. Suh J, Choi SH, Romano DM, Gannon MA, Lesinski AN, Kim DY, and Tanzi RE (2013). ADAM10 missense mutations potentiate β-amyloid accumulation by impairing prodomain chaperone function. Neuron 80, 385–401. 10.1016/j.neuron.2013.08.035. [PubMed: 24055016]
19. Anders A, Gilbert S, Garten W, Postina R, and Fahrenholz F (2001). Regulation of the α-secretase ADAM10 by its prodomain and proprotein convertases. FASEB J. 15, 1837–1839. 10.1096/fj.01-0007fje. [PubMed: 11481247]
20. Seegar TCM, Killingsworth LB, Saha N, Meyer PA, Patra D, Zimmerman B, Janes PW, Rubinstein E, Nikolov DB, Skiniotis G, et al. (2017). Structural Basis for Regulated Proteolysis by the α-Secretase ADAM10. Cell 171, 1638–1648.e7. 10.1016/j.cell.2017.11.014. [PubMed: 29224781]
21. Hemler ME (2005). Tetraspanin functions and associated microdomains. Nat. Rev. Mol. Cell Biol 6, 801–811. 10.1038/nrm1736. [PubMed: 16314869]
22. Harrison N, Koo CZ, and Tomlinson MG (2021). Regulation of ADAM10 by the TspanC8 Family of Tetraspanins and Their Therapeutic Potential. Int. J. Mol. Sci 22, 6707. 10.3390/ijms22136707. [PubMed: 34201472]
23. Dornier E, Coumailleau F, Ottavi J-F, Moretti J, Boucheix C, Mauduit P, Schweisguth F, and Rubinstein E (2012). TspanC8 tetraspanins regulate ADAM10/Kuzbanian trafficking and promote Notch activation in flies and mammals. J. Cell Biol 199, 481–496. 10.1083/jcb.201201133. [PubMed: 23091066]
24. Haining EJ, Yang J, Bailey RL, Khan K, Collier R, Tsai S, Watson SP, Frampton J, Garcia P, and Tomlinson MG (2012). The TspanC8 Subgroup of Tetraspanins Interacts with A Disintegrin and Metalloprotease 10 (ADAM10) and Regulates Its Maturation and Cell Surface Expression*. J. Biol. Chem 287, 39753–39765. 10.1074/jbc.M112.416503. [PubMed: 23035126]
25. Shah J, Rouaud F, Guerrera D, Vasileva E, Popov LM, Kelley WL, Rubinstein E, Carette JE, Amieva MR, and Citi S (2018). A Dock-and-Lock Mechanism Clusters ADAM10 at Cell-Cell Junctions to Promote α-Toxin Cytotoxicity. Cell Rep. 25, 2132–2147.e7. 10.1016/j.celrep.2018.10.088. [PubMed: 30463011]
26. Noy PJ, Yang J, Reyat JS, Matthews AL, Charlton AE, Furmston J, Rogers DA, Rainger GE, and Tomlinson MG (2016). TspanC8 Tetraspanins and A Disintegrin and Metalloprotease 10 (ADAM10) Interact via Their Extracellular Regions: EVIDENCE FOR DISTINCT BINDING MECHANISMS FOR DIFFERENT TspanC8 PROTEINS. J. Biol. Chem 291, 3145–3157. 10.1074/jbc.M115.703058. [PubMed: 26668317]
27. Lipper CH, Gabriel K-H, Seegar TCM, Dürr KL, Tomlinson MG, and Blacklow SC (2022). Crystal structure of the Tspan15 LEL domain reveals a conserved ADAM10 binding site. Structure 30, 206–214.e4. 10.1016/j.str.2021.10.007. [PubMed: 34739841]
28. Jouannet S, Saint-Pol J, Fernandez L, Nguyen V, Charrin S, Boucheix C, Brou C, Milhiet P-E, and Rubinstein E (2016). TspanC8 tetraspanins differentially regulate the cleavage of ADAM10 substrates, Notch activation and ADAM10 membrane compartmentalization. Cell. Mol. Life Sci 73, 1895–1915. 10.1007/s00018-015-2111-z. [PubMed: 26686862]
29. Seipold L, Altmeppen H, Koudelka T, Tholey A, Kasparek P, Sedlacek R, Schweizer M, Bär J, Mikhaylova M, Glatzel M, et al. (2018). In vivo regulation of the A disintegrin and metalloproteinase 10 (ADAM10) by the tetraspanin 15. Cell. Mol. Life Sci 75, 3251–3267. 10.1007/s00018-018-2791-2. [PubMed: 29520422]

30. Prox J, Willenbrock M, Weber S, Lehmann T, Schmidt-Arras D, Schwanbeck R, Saftig P, and Schwake M (2012). Tetraspanin15 regulates cellular trafficking and activity of the ectodomain sheddase ADAM10. Cell. Mol. Life Sci 69, 2919–2932. 10.1007/s00018-012-0960-2. [PubMed: 22446748]

31. Eschenbrenner E, Jouannet S, Clay D, Chaker J, Boucheix C, Brou C, Tomlinson MG, Charrin S, and Rubinstein E (2020). TspanC8 tetraspanins differentially regulate ADAM10 endocytosis and half-life. Life Sci. Alliance 3, e201900444. 10.26508/lsa.201900444. [PubMed: 31792032]

32. Noy PJ, Yang J, Reyat JS, Matthews AL, Charlton AE, Furmston J, Rogers DA, Rainger GE, and Tomlinson MG (2016). TspanC8 Tetraspanins and A Disintegrin and Metalloprotease 10 (ADAM10) Interact via Their Extracellular Regions. J. Biol. Chem 291, 3145–3157. 10.1074/jbc.M115.703058. [PubMed: 26668317]

33. Hiroshima K, Shiiba M, Oka N, Hayashi F, Ishida S, Fukushima R, Koike K, Iyoda M, Nakashima D, Tanzawa H, et al. (2019). Tspan15 plays a crucial role in metastasis in oral squamous cell carcinoma. Exp. Cell Res 384, 111622. 10.1016/j.yexcr.2019.111622. [PubMed: 31518558]

34. Zhang B, Zhang Z, Li L, Qin Y-R, Liu H, Jiang C, Zeng T-T, Li M-Q, Xie D, Li Y, et al. (2018). TSPAN15 interacts with BTRC to promote oesophageal squamous cell carcinoma metastasis via activating NF-κB signaling. Nat. Commun 9, 1423. 10.1038/s41467-018-03716-9. [PubMed: 29650964]

35. Jumper J, Evans R, Pritzel A, Green T, Figurnov M, Ronneberger O, Tunyasuvunakool K, Bates R, Žídek A, Potapenko A, et al. (2021). Highly accurate protein structure prediction with AlphaFold. Nature 596, 583–589. 10.1038/s41586-021-03819-2. [PubMed: 34265844]

36. Umeda R, Satouh Y, Takemoto M, Nakada-Nakura Y, Liu K, Yokoyama T, Shirouzu M, Iwata S, Nomura N, Sato K, et al. (2020). Structural insights into tetraspanin CD9 function. Nat. Commun 11, 1606. 10.1038/s41467-020-15459-7. [PubMed: 32231207]

37. Yang Y, Liu XR, Greenberg ZJ, Zhou F, He P, Fan L, Liu S, Shen G, Egawa T, Gross ML, et al. (2020). Open conformation of tetraspanins shapes interaction partner networks on cell membranes. EMBO J. 39, e105246. 10.15252/embj.2020105246. [PubMed: 32974937]

38. Zimmerman B, Kelly B, McMillan BJ, Seegar TCM, Dror RO, Kruse AC, and Blacklow SC (2016). Crystal Structure of a Full-Length Human Tetraspanin Reveals a Cholesterol-Binding Pocket. Cell 167, 1041–1051.e11. 10.1016/j.cell.2016.09.056. [PubMed: 27881302]

39. Susa KJ, Rawson S, Kruse AC, and Blacklow SC (2021). Cryo-EM structure of the B cell co-receptor CD19 bound to the tetraspanin CD81. Science 371, 300–305. 10.1126/science.abd9836. [PubMed: 33446559]

40. Koo CZ, Harrison N, Noy PJ, Szyroka J, Matthews AL, Hsia H-E, Müller SA, Tüshaus J, Goulding J, Willis K, et al. (2020). The tetraspanin Tspan15 is an essential subunit of an ADAM10 scissor complex. J. Biol. Chem 295, 12822–12839. 10.1074/jbc.RA120.012601. [PubMed: 32111735]

41. Uemura K, Kihara T, Kuzuya A, Okawa K, Nishimoto T, Ninomiya H, Sugimoto H, Kinoshita A, and Shimohama S (2006). Characterization of sequential N-cadherin cleavage by ADAM10 and PS1. Neurosci. Lett 402, 278–283. 10.1016/j.neulet.2006.04.018. [PubMed: 16687212]

42. Matthews AL, Szyroka J, Collier R, Noy PJ, and Tomlinson MG (2017). Scissor sisters: regulation of ADAM10 by the TspanC8 tetraspanins. Biochem. Soc. Trans 45, 719–730. 10.1042/BST20160290. [PubMed: 28620033]

43. Koo CZ, Matthews AL, Harrison N, Szyroka J, Nieswandt B, Gardiner EE, Poulter NS, and Tomlinson MG (2022). The Platelet Collagen Receptor GPVI Is Cleaved by Tspan15/ADAM10 and Tspan33/ADAM10 Molecular Scissors. Int. J. Mol. Sci 23, 2440. 10.3390/ijms23052440. [PubMed: 35269584]

44. Weskamp G, Ford JW, Sturgill J, Martin S, Docherty AJP, Swendeman S, Broadway N, Hartmann D, Saftig P, Umland S, et al. (2006). ADAM10 is a principal “sheddase” of the low-affinity immunoglobulin E receptor CD23. Nat. Immunol 7, 1293–1298. 10.1038/ni1399. [PubMed: 17072319]

45. Loganathan SK, Schleicher K, Malik A, Quevedo R, Langille E, Teng K, Oh RH, Rathod B, Tsai R, Samavarchi-Tehrani P, et al. (2020). Rare driver mutations in head and neck squamous cell carcinomas converge on NOTCH signaling. Science 367, 1264–1269. 10.1126/science.aax0902. [PubMed: 32165588]

46. Liu PCC, Liu X, Li Y, Covington M, Wynn R, Huber R, Hillman M, Yang G, Ellis D, Marando C, et al. (2006). Identification of ADAM10 as a major source of HER2 ectodomain sheddase activity in HER2 overexpressing breast cancer cells. Cancer Biol. Ther 5, 657–664. 10.4161/cbt.5.6.2708. [PubMed: 16627989]
47. Wetzel S, Seipold L, and Saftig P (2017). The metalloproteinase ADAM10: A useful therapeutic target? Biochim. Biophys. Acta BBA - Mol. Cell Res 1864, 2071–2081. 10.1016/j.bbamcr.2017.06.005.
48. Susa KJ, Seegar TC, Blacklow SC, and Kruse AC (2020). A dynamic interaction between CD19 and the tetraspanin CD81 controls B cell co-receptor trafficking. eLife 9, e52337. 10.7554/eLife.52337. [PubMed: 32338599]
49. Liu C, Xu P, Lamouille S, Xu J, and Derynck R (2009). TACE-mediated ectodomain shedding of the type I TGF-beta receptor downregulates TGF-beta signaling. Mol. Cell 35, 26–36. 10.1016/j.molcel.2009.06.018. [PubMed: 19595713]
50. Morin A, Eisenbraun B, Key J, Sanschagrin PC, Timony MA, Ottaviano M, and Sliz P (2013). Collaboration gets the most out of software. eLife 2, e01456. 10.7554/eLife.01456. [PubMed: 24040512]
51. Mastronarde DN (2005). Automated electron microscope tomography using robust prediction of specimen movements. J. Struct. Biol 152, 36–51. 10.1016/j.jsb.2005.07.007. [PubMed: 16182563]
52. Punjani A, Rubinstein JL, Fleet DJ, and Brubaker MA (2017). cryoSPARC: algorithms for rapid unsupervised cryo-EM structure determination. Nat. Methods 14, 290–296. 10.1038/nmeth.4169. [PubMed: 28165473]
53. Sanchez-Garcia R, Gomez-Blanco J, Cuervo A, Carazo JM, Sorzano COS, and Vargas J (2021). DeepEMhancer: a deep learning solution for cryo-EM volume post-processing. Commun. Biol 4, 1–8. 10.1038/s42003-021-02399-1. [PubMed: 33398033]
54. Pettersen EF, Goddard TD, Huang CC, Couch GS, Greenblatt DM, Meng EC, and Ferrin TE (2004). UCSF Chimera--a visualization system for exploratory research and analysis. J. Comput. Chem 25, 1605–1612. 10.1002/jcc.20084. [PubMed: 15264254]
55. Afonine PV, Grosse-Kunstleve RW, Echols N, Headd JJ, Moriarty NW, Mustyakimov M, Terwilliger TC, Urzhumtsev A, Zwart PH, and Adams PD (2012). Towards automated crystallographic structure refinement with phenix.refine. Acta Crystallogr. D Biol. Crystallogr 68, 352–367. 10.1107/S0907444912001308. [PubMed: 22505256]
56. Emsley P, and Cowtan K (2004). Coot: model-building tools for molecular graphics. Acta Crystallogr. D Biol. Crystallogr 60, 2126–2132. 10.1107/S0907444904019158. [PubMed: 15572765]
57. Schrödinger L (2010). The PyMOL Molecular Graphics System, Version 2.5.1.

Highlights

- Atomic model for an ADAM10-Tetraspanin 15 complex determined by cryo-EM
- Structure reveals primary and secondary interfaces
- Primary interface is responsible for complex formation and relief of autoinhibition
- Secondary interface positions active site for membrane-proximal substrate cleavage

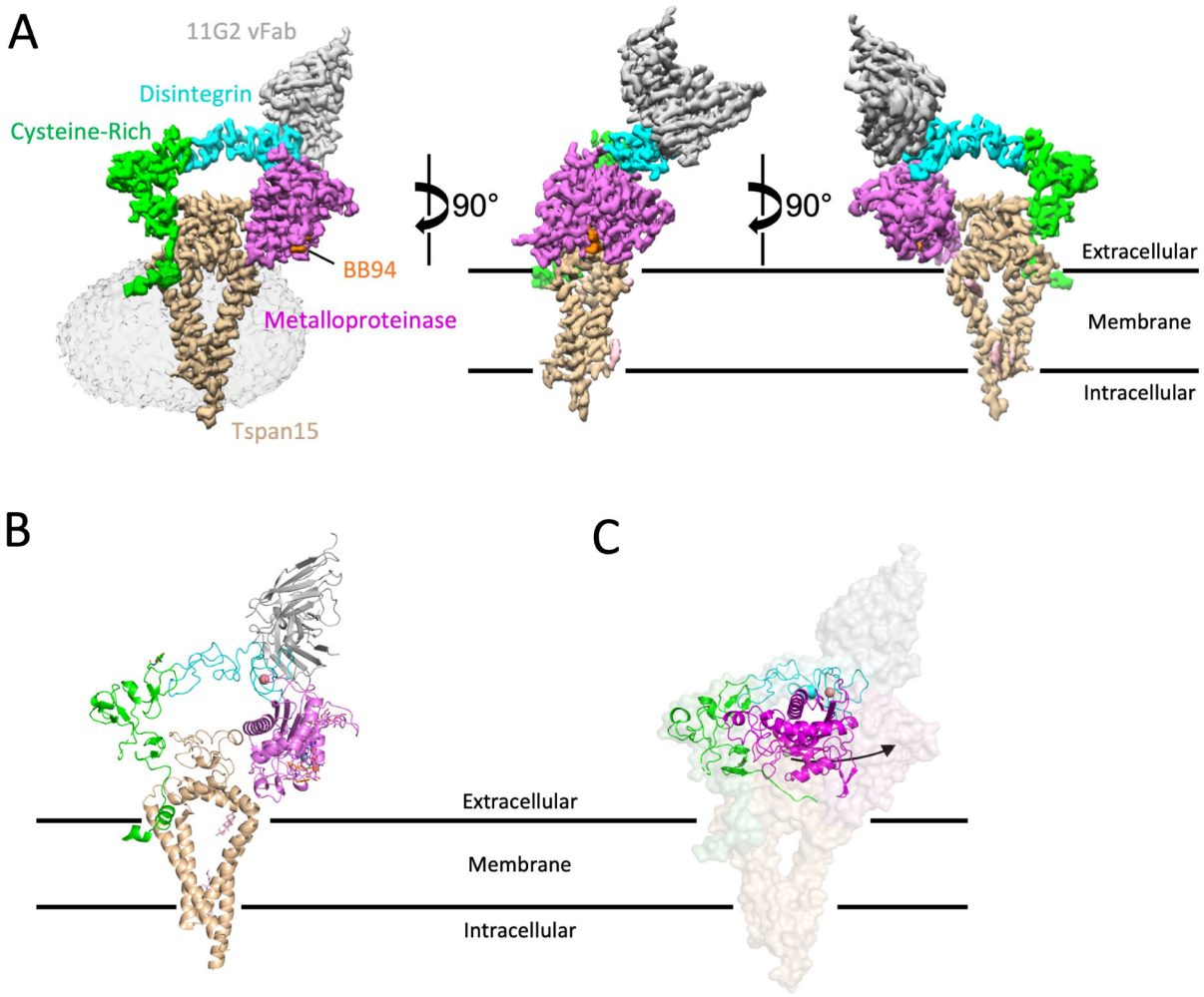

Figure 1. Structure of the ADAM10-Tspan15 complex.

A. Different views of the cryo-EM electron density map of the vFab-ADAM10-Tspan15 complex. The density associated with the detergent micelle is rendered transparently in the left panel. Tspan15 is beige, the 11G2 vFab is gray, the BB94 inhibitor is orange, and the catalytic, disintegrin, and cysteine-rich domains of ADAM10 are magenta, cyan and green, respectively. **B**. Cartoon representation of the complex, using the same color scheme. The zinc ion at the active site is represented as a gray sphere, and the bound calcium ion in the disintegrin domain is orange. **C**. Comparison of the free ADAM10 ectodomain (ribbon) with ADAM10 in the vFab-ADAM10-Tspan15 complex (surface). See also Figures S1–S3, Table 1, and Supplementary Video S1.

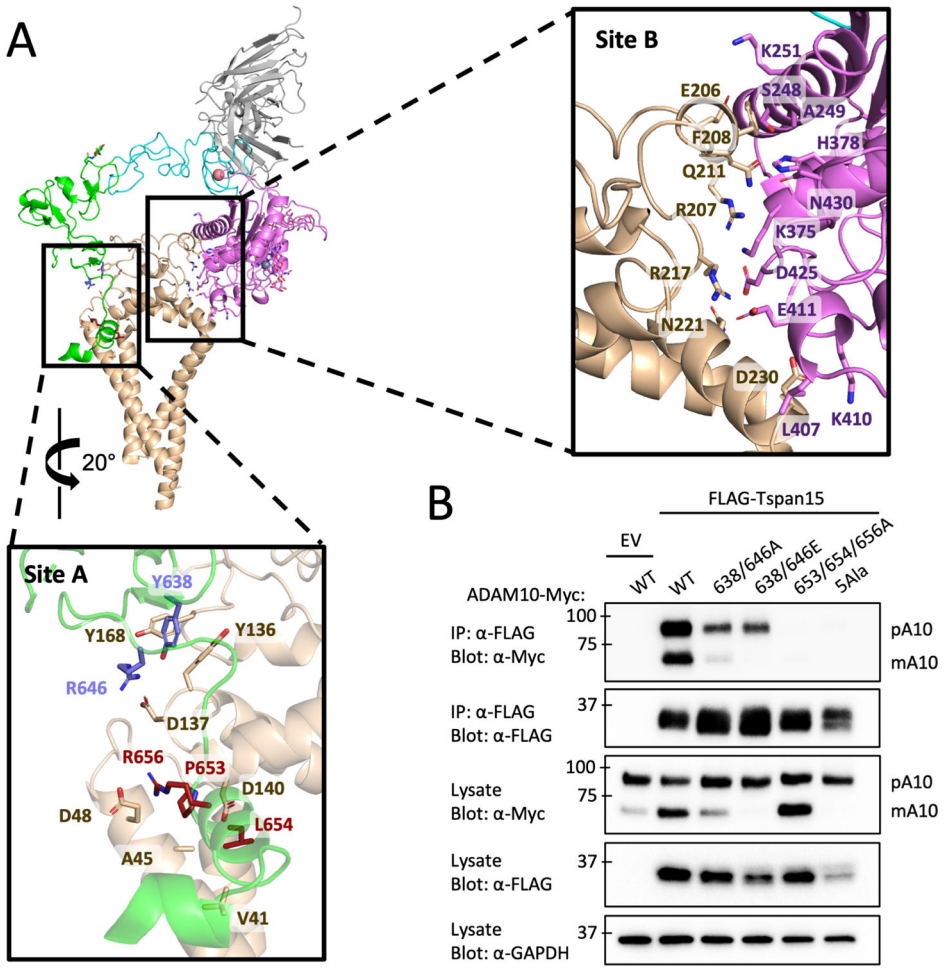

Figure 2. ADAM10-Tspan15 contact interfaces and mutational analysis.

(A) Cartoon representation of the vFab-ADAM10-Tspan15 complex with site A (left) and site B (right) interfaces boxed. A close-up view of the interface at site A is shown below the main panel, and a close-up view of the site B interface is shown to the right. The two clusters of interface A residues mutated in the immunoprecipitation assays are shown in blue and maroon. (B) Effect of ADAM10 mutations on co-immunoprecipitation with Tspan15. HEK293 cells were co-transfected with wild-type or mutant ADAM10-myc and FLAG-Tspan15 or vector control, and cell lysates were immunoprecipitated with anti-FLAG antibodies. The lysates and immunoprecipitates were subjected to SDS-PAGE, and analyzed by western blot using anti-myc or anti-FLAG antibodies. Lysates were also probed with an anti-GAPDH antibody (bottom) as a loading control. See also Figure S4.

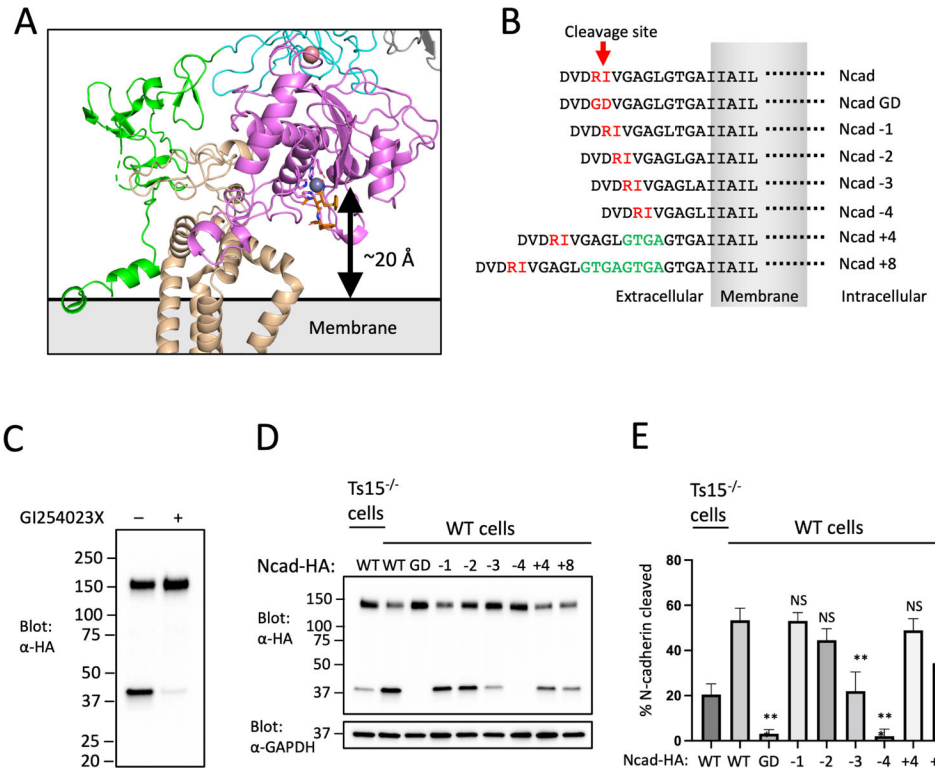

Figure 3. Analysis of the dependence of substrate cleavage on the distance of the scissile bond from the membrane.

(A) Zoomed-in view of the ADAM10 active site and its position relative to the membrane. The active site residues are shown in magenta sticks, the catalytic Zn^{++} ion is a gray sphere, and the BB94 hydroxamic acid inhibitor is rendered in orange sticks. (B) Design of N-cadherin (Ncad) variants for the substrate cleavage assay, and nomenclature used to name the substrate variants. (C) ADAM10 dependence of N-cadherin cleavage. U251 cells were transfected with Ncad containing an HA tag it its C-terminal end, and either mock treated or treated with the ADAM10 inhibitor GI254023X. Cell lysates were subjected to SDS-PAGE, and analyzed by Western blot using an anti-HA antibody. (D) N-cadherin substrate cleavage assay. Parental or Tspan15 knockout ($Ts15^{-/-}$) U251 cells were transfected with one of the HA-tagged Ncad variants shown in panel B. Cells were lysed after 48 hours and blotted with an anti-HA antibody to determine the extent of cleavage. Lysates were also blotted with anti-GAPDH (bottom) as a loading control. Data are representative of three independent biological replicates. (E) Quantification of N-cadherin cleavage using the Western blot results from all replicates. Blots were quantified using ImageJ software. Error bars indicate mean ± standard deviation of three independent experiments. Statistical analysis was performed in GraphPad Prism 7 using an unpaired t test (two-tailed). * $p< 0.05$; ** $p<0.01$; *** $p<0.001$. See also Figure S5.

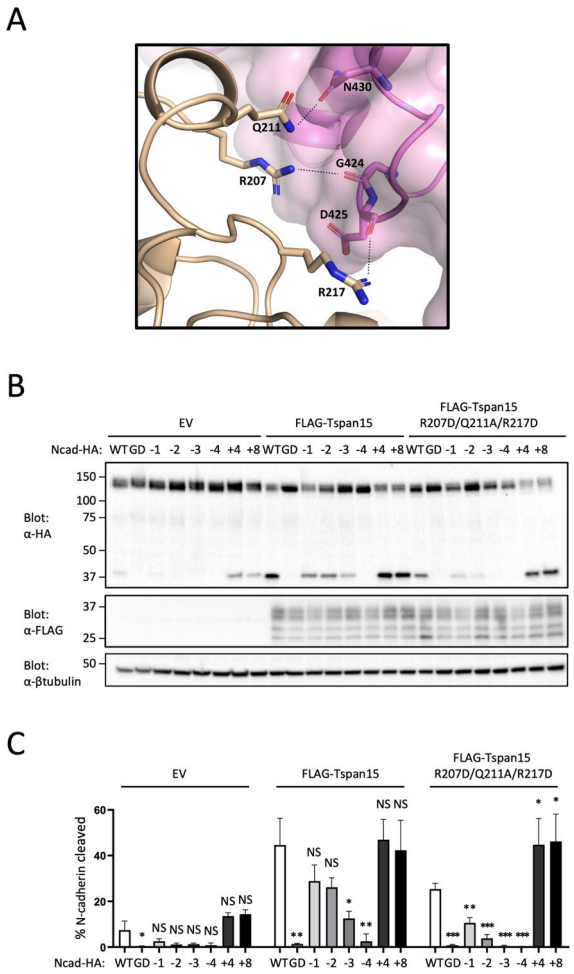

Figure 4. Analysis of the Tspan15-catalytic domain (site B) interface.

(A) View of the ADAM10-Tspan15 complex highlighting the residues mutated at the site B interface. Tspan15 is shown in beige, and that catalytic domain of ADAM10 is shown in magenta. Side chains of Tspan15 interface residues that were mutated (R207D, Q211A, and R217D) are shown as sticks. ADAM10 residues shown as sticks are within H-bonding distance (dashed lines) of Tspan15. (B) N-cadherin cleavage assay analyzing the Tspan15 site B interface mutant. Tspan15 knockout U251 cells were transfected with vector control (EV), FLAG-tagged wild-type Tspan15 or the Tspan15 site B interface mutant, and with one of the HA-tagged Ncad variants. Cells were lysed after 48 hours, and blotted with anti-HA to determine the extent of cleavage, and with anti-FLAG to confirm Tspan15 protein expression. Lysates were also blotted with anti-β-tubulin (bottom) as a loading control. Data are representative of three independent biological replicates. (C) Quantification of N-cadherin cleavage using the Western blot results from all replicates. Blots were quantified using ImageJ software. Error bars indicate mean ± standard deviation of three independent experiments. Statistical analysis was performed in GraphPad Prism 7 using an unpaired t test (two-tailed). * $p < 0.05$; ** $p<0.01$; *** $p<0.001$. See also Figure S5.

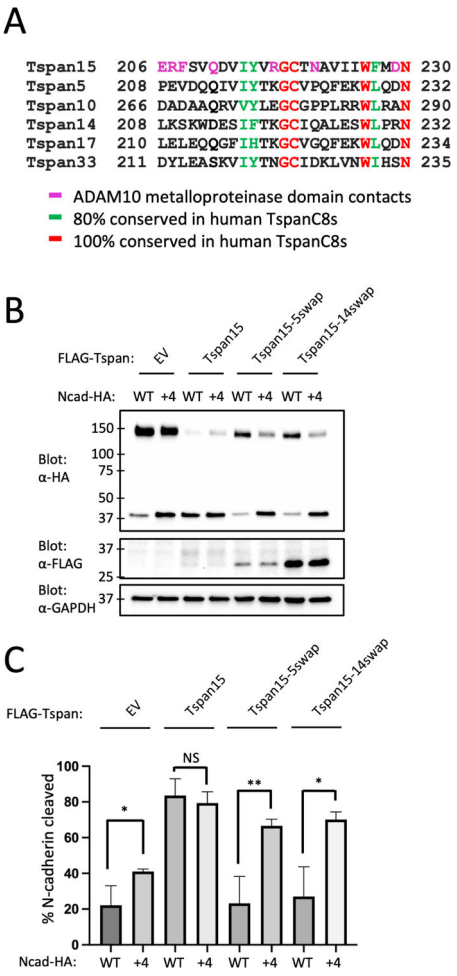

Figure 5. N-cadherin cleavage assay analyzing Tspan site B chimeras.

(A) Sequence alignment of the site B interface region of the six C8-tetraspanin proteins. (B). Tspan15 knockout U251 cells were transfected with vector control (EV), FLAG-tagged wild-type Tspan15, Tspan15/Tspan5, or Tspan15/Tspan14 chimeric proteins, and with either an HA-tagged Ncad or Ncad+4 variant. Cells were lysed after 48 hours, and blotted with anti-HA to determine the extent of cleavage, and with anti-FLAG to confirm Tspan protein expression. Lysates were also blotted with anti-GAPDH (bottom) as a loading control. Data are representative of three independent biological replicates. (C) Quantification of N-cadherin cleavage using the Western blot results from all replicates. Blots were quantified using ImageJ software. Error bars indicate mean ± standard deviation of three independent experiments. Statistical analysis was performed in GraphPad Prism 7 using an unpaired t test (two-tailed). * $p < 0.05$; ** $p<0.01$. See also Figure S5.

Table 1.

Data Collection and Refinement Statistics.

Data collection and processing	
Magnification	105,000
Voltage (kV)	300
Total dose (e–/Å^2)	51.99
Dose per physical pixel per second	27.22
Dose per Å^2 per second	39.993
Exposure time (s)	1.3
Number of frames	50
Dose per frame (e/Å^2)	1.04
Defocus range (μm)	−1.0 to −2.2
Pixel size (Å)	0.825
Symmetry	C1
Initial particle images	1822048
Final particle images	178031
Map resolution (Å) FSC	3.3
Threshold	(0.143)
Refinement	
Model composition	
Non-hydrogen atoms	7222
Protein residues	933
Ligands	13
B-factors (Å^2)	
Protein	56.68
Ligands	68.31
R.m.s deviations	
Bond lengths (Å)	.003
Bond angles (°)	1.036
Validation	
MolProbity score	2.06
Clashscore	12.85
Rotamer outliers (%)	0
Ramachandran plot	
Favored (%)	93.07
Allowed (%)	6.72
Disallowed (%)	0.22

Key resources table

REAGENT or RESOURCE	SOURCE	IDENTIFIER
Antibodies		
Rabbit anti-FLAG	Cell Signaling Technology	Cat # 14793 RRID:AB_2572291
Rabbit anti-myc-tag (clone 71D10)	Cell Signaling Technology	Cat # 2278 RRID:AB_490778
Rabbit anti-GAPDH (clone 14C10)	Cell Signaling Technology	Cat # 2118s RRID:AB_561053
Mouse anti-β-tubulin (clone D3U1W)	Cell Signaling Technology	Cat # 86298S RRID: AB_2715541
Mouse anti-HA (clone 6E2)	Cell Signaling Technology	Cat # 2367 RRID:AB_ 10691311
Goat anti-rabbit-HRP	Abcam	Cat # ab6721
Goat anti-mouse-HRP	ThermoFisher	Cat # 62–6520
ANTI-FLAG M2 Affinity Gel	Sigma-Aldrich	Cat # A2220 RRID: AB_10063035
Chemicals, peptides, and recombinant proteins		
Batimastat (BB94)	Sigma-Aldrich	Cat # 19440
Compound E	EMD Millipore	Cat # 565790
Mca-PLAQAV-Dpa	R&D Systems	Cat # ES003
U251 Avalanche transfection reagent	EZ Biosystems	Cat # EZT-U251–1
PEI Max 40000	VWR	Cat # 75800–188
n-Dodecyl-b-D-Maltoside	Anatrace	Cat # D310
Cholesteryl hemisuccinate	Sigma-Aldrich	Cat # C6512
N-ethylmaleimide	Sigma-Aldrich	Cat # E3876
Expi293 expression medium	ThermoFisher	Cat # A1435103
HisPur Ni-NTA resin	ThermoFisher	Cat # 88222
Protein A agarose resin	EMD Millipore	Cat # 16–125
M1 anti-FLAG resin	Produced in-house	N/A
3C protease recombinant protein	Produced in-house	N/A
Critical commercial assays		
Western Lightning Plus-ECL detection Kit	PerkinElmer	Cat # NEL103001EA
Deposited data		
vFab-ADAM10-Tspan15 complex structure coordinates and EM density map	This paper	PDB: 8ESV EMDB: EMD-28580
ADAM10 ectodomain-11G2Fab complex structure coordinates	Seegar et al.[20]	PDB: 6BDZ
ADAM10 ectodomain structure coordinates	Seegar et al.[20]	PDB: 6BE6
Human Tspan15 LEL-1C12Fab structure coordinates	Lipper et al.[27]	PDB: 7RD5
CD9 structure coordinates	Umeda et al.[36]	PDB: 6K4J
CD53 structure coordinates	Yang et al.[37]	PDB: 6WVG
CD81 structure coordinates	Zimmerman et al.[38]	PDB: 5TCX
Experimental models: Cell lines		
HEK293T cells	ATCC	Cat # CRL-3216

REAGENT or RESOURCE	SOURCE	IDENTIFIER
Expi293F cells	ThermoFisher	Cat # A14527
U251 cells	Gift from Thomas M. Roberts at the Dana-Farber Cancer Institute	N/A
U251-Ts15−/− cells	Lipper et al.[27]	N/A
Recombinant DNA		
pcDNA3.1/Hygro(+)	ThermoFisher	Cat # V87020
pRK5M-ADAM10-myc	Liu et al.[49]	Addgene Cat # 31717
pFUSE-hIgG1-Fc2	Invivogen	Cat # pfuse-hg1fc2
gBlocks	Integrated DNA Technologies	N/A
Software and Algorithms		
SBGrid Consortium	Morin et al.[50]	https://sbgrid.org
SerialEM	Mastronarde[51]	https://bio3d.colorado.edu/SerialEM/
cryoSPARC	Structura Biotechnology Inc.[52]	https://cryosparc.com
DeepEMhancer	Sanchez-Garcia et al.[53]	https://github.com/rsanchezgarc/deepEMhancer/
UCSF Chimera	Pettersen et al.[54]	https://www.rbvi.ucsf.edu/chimera/
Phenix	Afonine et al.[55]	https://www.phenix-online.org
Coot	Emsley and Cowtan[56]	https://www2.mrc-lmb.cam.ac.uk/personal/pemsley/coot/
Pymol	Schrödinger[57]	https://pymol.org/2/
Other		
Quantifoil 400 mesh copper grids R 1.2/1.3	Electron Microscopy Sciences	Q4100CR1.3